Numerical methods and failure mechanisms of ferrofluid seals in centrifugal pumps

Wangxu Li[1], Hongliang Li[1], Zhenggui Li[1,2*], Wei Han[1,3], Rennian Li[1], Yue Zhang[1]

(1. *School of Energy and Power Engineering, Lanzhou University of Technology, Lanzhou 730050, China*;
2. *School of Engineering, Qinghai Institute of Technology, Xining 810016, China*;
3. *School of Green Energy and Energy Storage, Lanzhou University of Technology, Lanzhou 730050, China*)

Abstract: Ferrofluid seals are considered a next-generation sealing technology for hydraulic machinery due to their outstanding performance. However, experiments and engineering applications have revealed issues with seal failure, the mechanisms of which remain poorly understood. This study focuses on centrifugal pumps, employing numerical simulations to analyze the hydrodynamic characteristics and pressure pulsations in the sealing clearance. A coupling interface between the three-dimensional fluid machinery numerical results and two-dimensional ferrofluid seal numerical results was established to investigate the effects of mean and pulsating pressures on the ferrofluid interface morphology and the mechanisms of seal failure. The results indicate that the rotation of the centrifugal pump shaft induces forced vortices in the sealing clearance. Influenced by the clearance structure, these forced vortices generate free vortices with similar flow patterns. The vortex motion is identified as the primary factor causing pressure pulsations in the sealing clearance, with an amplitude of approximately 0.18 MPa due to scale limitations. Compared to the morphology of ferrofluid seals under mean pressure, pulsating flow does not cause partial detachment of the ferrofluid but accelerates the rupture process of the ferrofluid sealing ring. Under the critical pressure of the ferrofluid sealing ring, pulsating pressure causes significant damage within 0.8 s. This study concludes that the stability and failure of ferrofluid seals in centrifugal pumps are strongly governed by vortex-induced pressure fluctuations and the interaction between magnetic field distribution and flow dynamics. The designed four-level ferrofluid sealing device can effectively withstand peak pressure pulsations, demonstrating reliable sealing performance. These findings provide critical insights for optimizing ferrofluid seal designs and can guide the development of more reliable sealing technologies in high-speed hydraulic machinery, improving operational safety and efficiency.

Keywords: hydraulic machinery, ferrofluid seal, multi-field coupling, failure mechanism

DOI: 10.25165/j.ijabe.20261902.10146

Citation: Li W X, Li H L, Li Z G, Han W, Li R N, Zhang Y. Numerical methods and failure mechanisms of ferrofluid seals in centrifugal pumps. Int J Agric & Biol Eng, 2026; 19(2): 183–192.

1 Introduction

The traditional sealing devices for centrifugal pumps have exposed a number of reliability issues stemming from structural and sealing principle limitations. These include wear problems in the friction pairs of mechanical seals, as well as failures in the dynamic and static sealing rings[1]. Additionally, threaded seals experience leakage during low-speed operation and instability issues in the rotor caused by radial excitation forces from fluid in small gaps[2]. Packing seals also face challenges such as friction loss during high-speed operation of centrifugal pump shafts and degradation of the soft packing due to frictional heat[3]. These long-standing sealing problems have not been fundamentally resolved, and the limitations of centrifugal pump shaft sealing technology hinder its development towards higher speeds, larger flow rates, and greater efficiency. Therefore, the introduction of new sealing methods is imperative.

Ferrofluid, as a liquid medium that can be remotely controlled through a magnetic field[4-6], presents a new solution for addressing rotation sealing issues. By utilizing permanent magnets as the magnetic field source, a specially designed magnetic circuit can focus the magnetic field and create a gradient along the rotational axis. Under the influence of the dipole force $\mu_0 M\nabla H$ (where μ_0 is the permeability of free space, $4\pi\times10^{-7}$ H/m; M is the magnetization intensity of the magnetic fluid, and H is the magnetic field strength) between uniformly dispersed and dense nano ferromagnetic particles and the magnetic field, the magnetic fluid can be confined within the sealing gap, forming a magnetic pressure p_s that resists external forces and achieves sealing effects. Since it is a liquid seal, the wear between the magnetic fluid and solid structures is minimal, and it has good compatibility with solid wall structures, reducing the processing precision requirements of the sealing device while enhancing its reliability and stability[7-10]. Currently, magnetic fluid sealing has shown surprisingly effective results in practical applications such as dry rotary pumps[11] and tank perimeter viewing systems[12].

Despite the promise of ferrofluid sealed in dynamic sealing applications, some complex flow mechanisms that arise during the sealing of liquid media remain insufficiently understood, particularly the unstable behavior of liquid-liquid interfaces. In rotating machinery such as centrifugal pumps and water turbines, the pulsating flow fields induced by dynamic-static interference can

Received date: 2025-08-30 **Accepted date:** 2026-01-04

Biographies: Wangxu Li, Lecturer, research interest: ferrofluid application, Email: liwxu@lut.edu.cn; **Hongliang Li**, Postgraduate, research interest: ferrofluid seals, Email: 252080704015@lut.edu.cn; **Wei Han**, Professor, research interest: hydraulic machinery and theory of multiphase flow, Email: hanwei@lut.edu.cn; **Rennian Li**, Professor, research interest: hydraulic machinery and theory of multiphase flow, Email: lirn@lut.edu.cn; **Yue Zhang**, Lecturer, research interest: ferrofluid application, Email: 289368164@qq.com.

***Corresponding author: Zhenggui Li**, Professor, research interest: ferrofluid application. School of Energy and Power Engineering, Lanzhou University of Technology, Tel: +86-13919090195, Email: lzhgui@mail.xhu.edu.cn.

further trigger fluctuations at the magnetic fluid interface, accelerating seal failure. In recent years, extensive discussions have been held regarding ferrofluid sealing technology for rotating machinery like centrifugal pumps in liquid environments. Li et al.[13,14] explained how complex flow fields impact the sealing performance of ferrofluid from the perspective of cavitation in hydraulic machinery. The occurrence and intensification of cavitation phenomena enhance the magnitude and frequency of pressure fluctuations at the ferrofluid seal interface, leading to frequent microscale vibrations of the ferrofluid, which disrupt its cohesive forces and cause the surface ferrofluid to detach. Liu et al.[15] suggested that the velocity difference between the ferrofluid and the sealing medium induces detachment or rupture of the ferrofluid film. A new sealing structure with added barriers was proposed to compensate for the velocity differences, achieving good sealing of lubrication oil for over ten cycles at 1200 r/min and a sealing pressure of 3 kPa. Mitamura et al.[16] applied ferrofluid sealing with a barrier structure in blood pumps, achieving a reliable operational lifespan of continuous 275 d. Additionally, some studies have demonstrated the feasibility of ferrofluid for sealing marine propellers[17-20].

However, these studies aim to enhance the sealing performance or lifespan of ferrofluid through certain means without revealing the failure mechanisms of ferrofluid in liquid environments. This has led to existing technologies and theories being unable to fundamentally solve the sealing issues. Li et al.[21] designed a transparent ferrofluid sealing device and used an endoscope to document the entire failure process of the magnetic fluid during sealing operations, providing relatively comprehensive experimental data on ferrofluid failure mechanisms. Qian et al.[22] derived the velocity distribution rules between ferrofluid and sealing media based on the Navier-Stokes equations, demonstrating the key issue of instability at the ferrofluid interface through theoretical formulas. Chen et al.[23] conducted a detailed discussion on the failure process of ferrofluid from a numerical calculation perspective. However, these studies all employed uniform pressure as boundary conditions, which disconnects from the real pulsating flow fields inside hydraulic machinery such as centrifugal pumps. Therefore, the revealed mechanisms and the obtained characteristics of magnetic fluid sealing film movement are not comprehensive. There is still a need for extensive theoretical, experimental, and numerical research aligned with practical engineering regarding the failure mechanisms of ferrofluid seals in hydraulic machinery. This should involve proposing critical issues affecting interface instability from a fluid dynamics perspective and developing core control and manufacturing technologies based on foundational theories.

This study focuses on centrifugal pumps, constructing a three-dimensional fluid domain model of the centrifugal pump that includes leakage channels. Through numerical algorithms, the flow characteristics of the leakage channel and the pressure fluctuation data at the sealing interface under various operating conditions are obtained. The transient pressure fluctuation data at the sealing interface is used as the initial boundary condition for the ferrofluid sealing numerical model. Coupled with magnetic field-flow field technology, a numerical investigation is conducted on the ferrofluid sealing interface and rupture mechanisms influenced by pressure fluctuations. The relevant results fill the research gap regarding the motion characteristics of ferrofluid sealing interfaces under dynamic pressure effects while revealing the rupture mechanisms of ferrofluid seals in hydraulic machinery. This provides reference for optimizing control strategies for sealing devices. Figure 1 illustrates the relevant technical roadmap of this study.

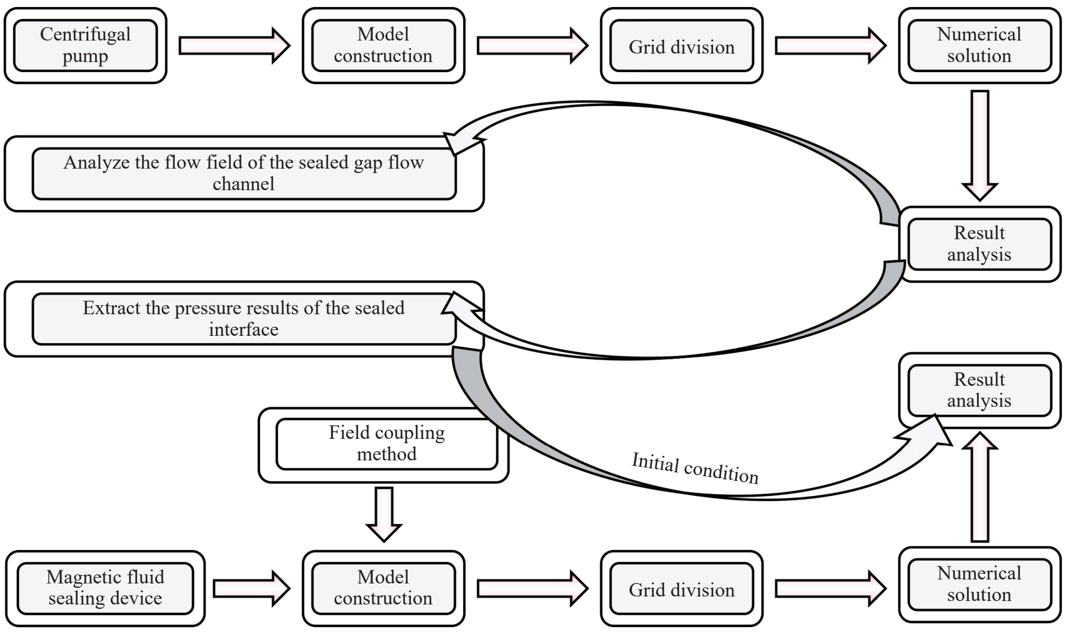

Figure 1 Numerical simulation and field-coupling technical route for centrifugal pump and ferrofluid sealing device

2 Materials and methods

This study is based on a centrifugal pump (model pump) and establishes a fluid domain model that includes the inlet flow area, outlet ring, impeller, volute, leakage channel, and sealing end face. The pump inlet diameter is 63 mm, the pump outlet diameter is 48 mm, the impeller inlet diameter is 80 mm, and the impeller outlet diameter is 140 mm, with a rated head H_d of 20 m, a rated flow rate Q_d of 50.6 m^3/h, a rated speed n_d of 2910 r/min, and six blades (Z). The shaft diameter is 36 mm. Detailed information regarding the model can be found in Figure 2.

The numerical research is conducted using Fluent software, with ICEM used to draw structured grids for the entire flow domain, providing conditions to capture more intricate flow details. Figure 3 illustrates the working principle of magnetic fluid sealing.

In the numerical calculations, the inlet of the centrifugal pump is set as a pressure inlet, while the outlet is configured as a flow rate outlet, using experimental data as the initial boundary conditions. The inlet pressure and outlet flow values for various flow conditions of the centrifugal pump are listed in Table 1. To ensure that the rotation of the flow domain is consistent with actual conditions, the steady-state calculations employ the Multiple Reference Frame (MRF) model, while the transient calculations utilize the sliding mesh (Mesh Motion) model. The impeller surface is set to be stationary relative to the rotating domain, while the other wall surfaces are set to be absolutely stationary. Since the RNG k-ε turbulence model accounts for the effects of vortical motions on turbulence and improves the prediction accuracy of swirling flows, it is more suitable for simulating complex internal flows such as those inside centrifugal pumps[24-27]. Therefore, the RNG k-ε turbulence model is adopted in this study.

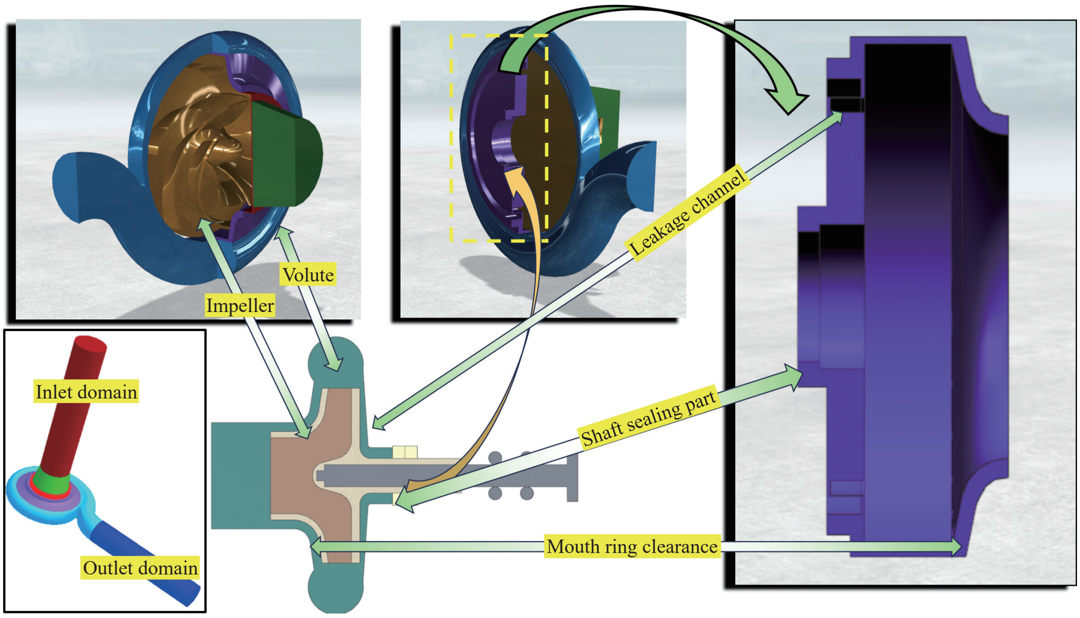

Figure 2 Structure diagram of the centrifugal pump

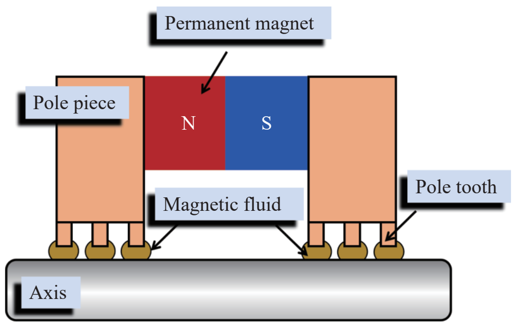

Figure 3 Principle of magnetic fluid sealing

Table 1 Inlet pressure and outlet flow values under various flow conditions

Q/Q_d	P_{in}	Q_{out}	Q/Q_d	P_{in}	Q_{out}
0.4	122 199	5.544	0.9	112 766	12.475
0.5	121 361	6.930	1.0	109 000	14.020
0.6	119 230	8.316	1.1	106 918	15.524
0.7	117 678	9.023	1.2	103 006	16.910
0.8	116 133	11.089	1.3	97 838	18.297

Note: Q represents the current flow rate in kg/m³, P_{in} indicates the inlet pressure in Pa, and Q_{out} denotes the outlet flow rate in kg/m³.

To verify the grid independence of the numerical calculations, different grid topologies and quantities are used as variable parameters to observe the variations in pump head. The relevant data is presented in Table 2. When the total number of grids exceeds 2 317 541, the variation in the centrifugal pump's head is less than 0.3%, indicating that a grid count greater than this value meets the computational requirements. Figure 4 illustrates the structured grid of the centrifugal pump. The formula for calculating the pump head can be referenced in Equation (1)[28-30].

$$H = \frac{p_{out} - p_{in}}{\rho g} + \frac{v_{out} - v_{in}}{2g} + (Z_{out} - Z_{in}) \tag{1}$$

where, H is the pump head, m; p_{out} is the pump outlet pressure, Pa; p_{in} is the pump inlet pressure, Pa; v_{out} is the liquid velocity at the pump outlet, m/s; v_{in} is the liquid velocity at the pump inlet, m/s; z_{out} is the distance between the pump outlet and the reference plane, m; z_{in} is the distance between the pump inlet and the reference plane, m; ρ is the fluid density, kg/m³; and g is the acceleration due to gravity, m/s².

Table 2 Grid model parameters of centrifugal pump

Plan	Number of grids	Head/m
A	1 013 514	19.98
B	1 537 624	21.33
C	2 317 541	22.01
D	2 841 908	22.04
E	3 174 019	22.02

An external characteristic experiment was conducted on the model pump to validate the reliability of the numerical calculation results using the head and efficiency characteristics of the centrifugal pump. The experimental setup is an open-type test bench, equipped with pressure sensors at both the inlet and outlet of the centrifugal pump, as well as a turbine flow meter. The prime mover is an electric motor that drives the centrifugal pump through a torque sensor. Beneath the experimental platform, there is a water tank that provides water to the pump and collects the liquid discharged from the pump, forming a closed loop. During the experiment, flow conditions between 0.4 and 1.3 were selected for the centrifugal pump. After adjusting the operating conditions, no data was recorded temporarily until the flow stabilized, after which data collection commenced. Figure 5 compares the external characteristic data (head and efficiency) collected from the experiment with the data obtained from numerical calculations. Both the calculated head and efficiency values are higher than the experimental values. This phenomenon mainly occurs because solid surface effects, such as fluid obstruction and wear, were not considered during the numerical calculations. However, the trends in the calculated head and efficiency values of the centrifugal pump were consistent with the experimental results, with the maximum deviation in head being less than 3 m. Therefore, the numerical calculation results can be deemed reliable. The formula for calculating efficiency η is given in Equation (2)[31,32].

$$\eta = \frac{HQ_m g}{T\omega} \tag{2}$$

where, Q_m is the mass flow rate of the centrifugal pump, kg/s; T is the torque on the shaft, N·m; and ω is the angular velocity of the shaft, rad/s.

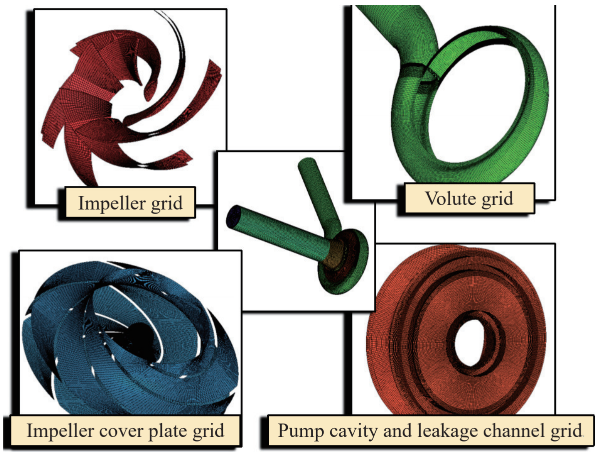

Figure 4 Grid model of the centrifugal pump

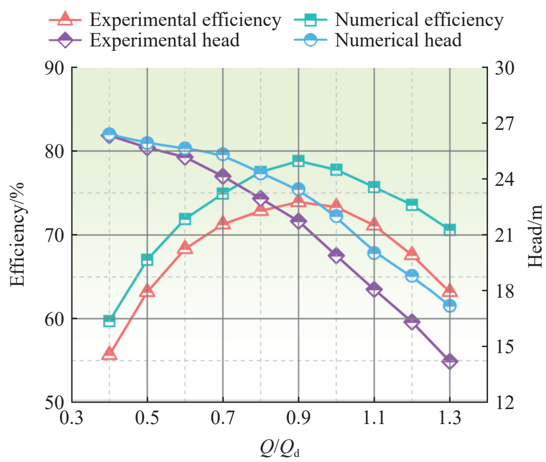

Figure 5 Reliability verification of numerical simulation for centrifugal pumps

3 Flow field analysis at the sealing gap of the centrifugal pump

3.1 The influence of flow conditions on the vortex motion characteristics at the clearance structure of centrifugal pumps

The vortex motion at the gap structure of the centrifugal pump is the fundamental cause of pressure fluctuations at the interface of the magnetic fluid seal, and it is also a key factor in the emulsification and failure of the magnetic fluid interface. To comprehensively analyze the characteristics of the vortex motion in the gap structure of the centrifugal pump, a flow range of 0.3-1.3 Q_d was selected to reveal the vortex motion mechanism using numerical methods. The axial slice along the x-direction of the centrifugal pump model was chosen as the display object, with the vorticity in the x-direction used as the physical quantity for visualizing the flow field.

Figure 6 shows the distribution patterns of vorticity, streamlines, and vortices in the sealing gap channel at flow rates of 0.3 Q_d, 0.7 Q_d, 1.0 Q_d, and 1.3 Q_d. During the rotation of the centrifugal pump's impeller, the rotating flow field superimposes with the parallel flow field to create a complex flow state. High-speed rotating fluid microgroups are generated within the impeller channel, which then flow towards the sealing channel under the influence of pressure differences. Due to the sudden reduction in cross-sectional area at the junction of the pump chamber gap and the sealing channel, the forced unstable flow converts to stable flow, thereby weakening the rotational motion of the fluid. Afterward, when the cross-sectional area expands again, the fluid disperses in a larger flow space. At 0.3 Q_d, the streamline at Position 1 shows slight curvature, with vorticity values ranging from 0 to 80 1/s, and the vortices appear to expand or become distorted. Based on the flow characteristics, it can be identified that the vortex in the gap channel at this moment is a free vortex, induced by changes in the state of the fluid itself. As the flow rate increases, more intense rotational motion occurs in the impeller region, transmitting vorticity downstream in the direction of flow. At this point, the micro-gap channel's stabilizing effect on high-intensity vortex movements cannot eliminate the rotational phenomenon of the fluid. At 0.7 Q_d, significant torque in the vortices appears, and at 1.0 Q_d, forced vortices emerge; by 1.3 Q_d, the flux and range of these forced vortices are further enhanced.

The fluid near the shaft surface is induced to form vortices due to the wall shear stress generated by the rotation of the main shaft. The vortices close to the shaft surface are thus forced vortices. In contrast, the fluid farther away from the shaft surface exhibits vortex structures induced by the forced vortices, with streamlines appearing divergent. Although there is a vorticity strength of 200 1/s, it can still be considered a free vortex. To substantiate this viewpoint, the vortex structure at Position 2 is selected, and the circumferential velocity values v_θ on either side of the vortex center are extracted. Since the numerical calculations employ a Cartesian coordinate system, v_θ needs to be transformed to obtain its values as represented in Equation (3).

$$v_\theta = v_y \cos\theta - v_x \sin\theta \tag{3}$$

where, v_x, v_y represent the velocity components of the liquid along the x and y directions (m/s) respectively, while θ denotes the angular parameter in the polar coordinate system, (°).

Figure 6 illustrates the variation pattern of v_θ along the radial direction from the vortex center at Position 3, providing evidence that v_θ is proportional to 1/r, aligning with the free vortex velocity distribution law.

During the vortex motion at Position 3, new induced vortices are generated at Position 2. However, the vortices at Position 2 are influenced by the vortices at Position 1, especially at high flow rates. When the vorticity generated by the impeller rotation cannot be eliminated through the gap channel, it imparts a stronger rotational torque on the vortices at Position 2. Consequently, the range of vortices at Position 2 is greater than that at Position 3. Moreover, as the flow rate increases, the interference of upstream fluid at Position 2 intensifies. At 1.3 Q_d, a single vortex at Position 2 splits into two vortices, enhancing the flow instability of the liquid at the sealing gap.

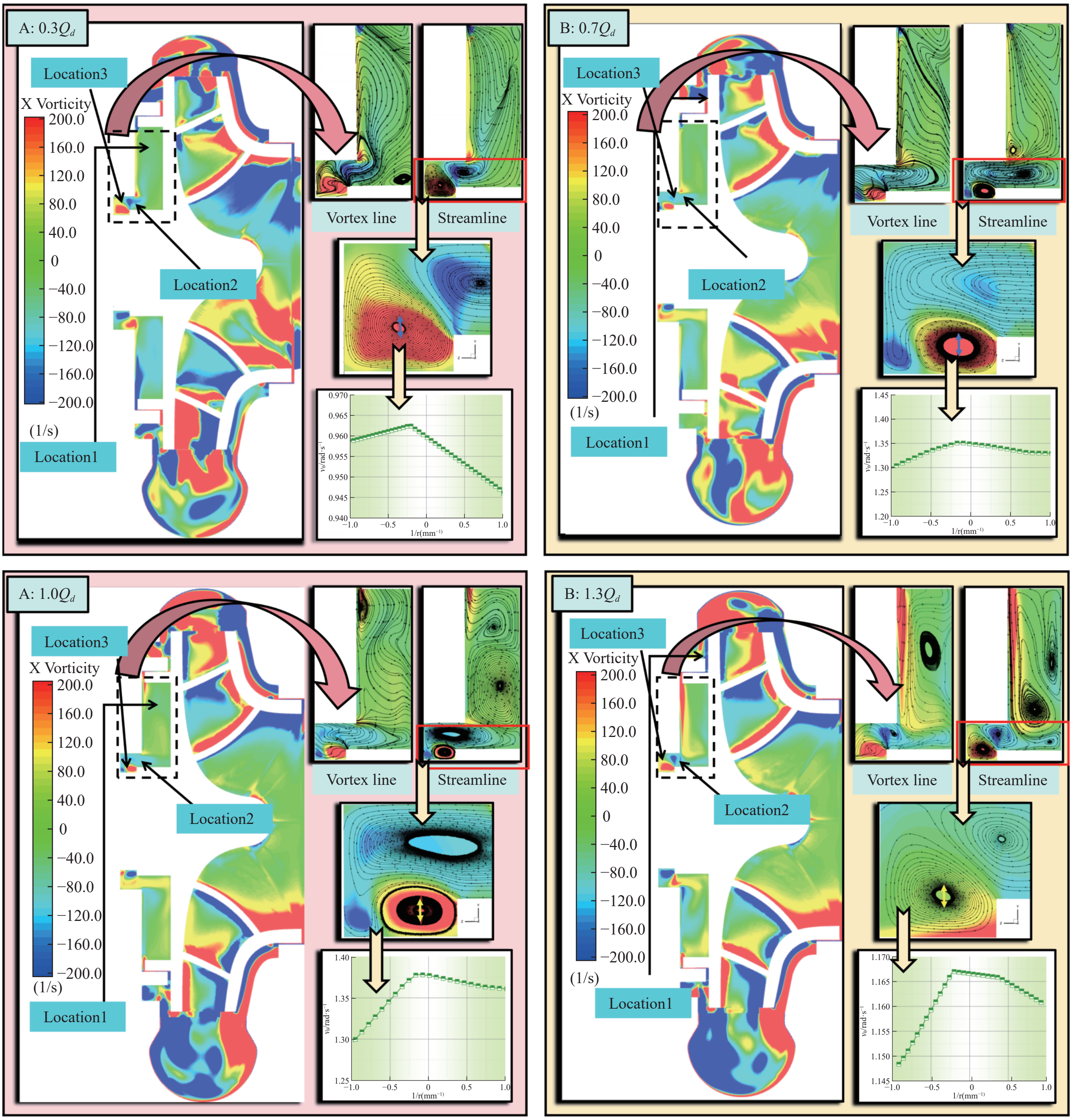

Figure 6 Vorticity distribution at the axial section of the centrifugal pump

3.2 Pressure pulsation characteristics at the ferrofluid sealing interface

Based on the vortex motion characteristics in the sealing gap, it can be concluded that the primary source of pressure pulsations at the interface of the magnetic liquid seal is the shearing action of the shaft surface on the liquid. To further explore the pressure pulsation characteristics of the magnetic liquid seal interface, three monitoring points near the sealing end are identified using a coordinate point localization method (as shown in Figure 7) to collect pressure data at the seal interface. Due to the relatively small radial distance of the ferrofluid seal interface, three uniformly distributed points were selected as the investigation locations.

In the numerical approach, the solver is set to transient, with the use of MRF transformed into Mesh Motion. The steady-state results serve as the initial conditions, and each rotation of the impeller is taken as a single time step, specifically every 3° of impeller movement. This results in a total of 1440 time steps, equivalent to 12 rotations of the impeller, with the numerical outcomes from the final four rotations serving as the sample data.

Figure 8 displays the pressure pulsation data at the ferrofluid seal interface under different flow conditions. At 0.3 Q_d, due to the small volume of liquid being transmitted within the pump body, the unstable flow created by vortices at the impeller is stabilized by the narrow gaps. However, the motion of the main shaft induces shear movement in the fluid at the gap, generating forced vortices along with free vortices that are induced by the forced vortices. As a result, the pressure pulsation amplitude at the proximity of the shaft (Position P1) is relatively high.

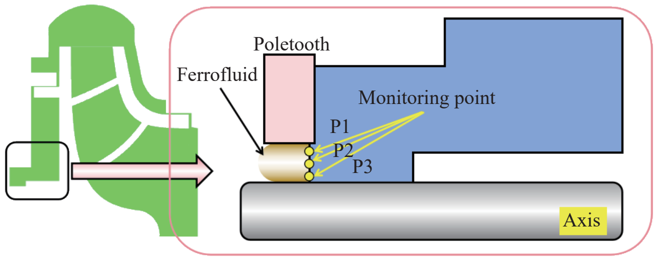

Figure 7 Position of pressure pulsation monitoring points

As the flow rate increases to 0.7 Q_d, the pressure pulsations at Positions P1, P2, and P3 on the ferrofluid seal interface become similar. At this point, the unstable flow generated by the impeller interferes with the seal interface and dominates the medium's pressure fluctuations, but the shear movement of the liquid induced by the shaft surface continues to contribute to the unstable flow. Therefore, the closer the position is to the shaft, the greater the amplitude of pressure pulsations.

With further increases in flow rate, the amplitudes of pressure pulsations at different interface positions become even more comparable; however, the flow rate directly influences the peak and trough values of pressure at the ferrofluid seal interface. Taking Position P1, where pressure pulsation is most intense, as an example, the peak pressure pulsation values at 0.3 Q_d, 0.7 Q_d, 1.0 Q_d, and 1.3 Q_d are 33.25×10^5 Pa, 30.99×10^5 Pa, 28.73×10^5 Pa, and 26.81×10^5 Pa, respectively. The trough values are 31.44 ×10^5 Pa, 28.73×10^5 Pa, 28.47×10^5 Pa, and 26.16×10^5 Pa, respectively. As the flow rate increases, both the peak and trough values of pressure pulsations gradually decrease. The pressure pulsation characteristics at low flow conditions can serve as reference pressures for the design of magnetic fluid sealing devices, ensuring that there are no issues with insufficient sealing pressure during other operating conditions.

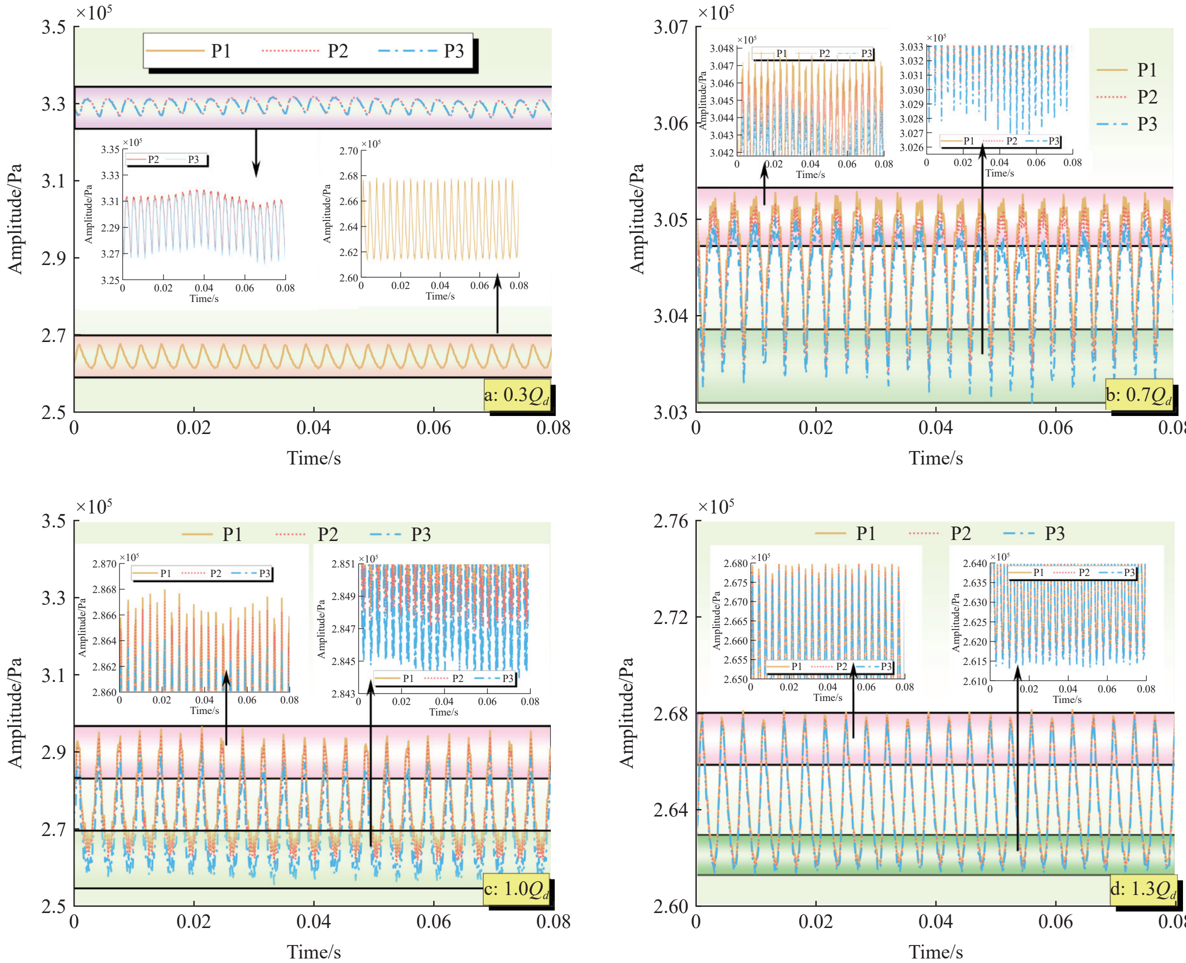

Figure 8 Results of pressure pulsation at the magnetic-liquid seal interface under different flow conditions

3.3 Design of ferrofluid sealing device for centrifugal pumps and magnetic field calculation

Referencing literature [11], the ratios of various parameters are defined as follows: the tooth width (L_t) to gap (L_g) ratio equals 5, the slot width (L_s) to L_g ratio is 20, and the tooth height (L_h) to L_s ratio is 1.25, with (L_g = 0.1) mm. More details can be found in Figure 1. Based on these proportions, the main parameters for designing the magnetic fluid sealing device are (L_t = 0.5) mm, (L_s = 2) mm, and (L_h = 2.5) mm. In the numerical calculations, the remanent magnetic induction intensity (B_r) of the permanent magnet (NdFeB) is set to 1.2 T, while the remaining ferromagnetic materials are made of electrical pure iron. The initial phase involves a four-level sealing device, with two pole teeth each on the left and right shoes. Because the magnetic permeability of the ferrofluid is close to that of air, all non-ferromagnetic parts are assigned air material in the numerical computations.

Figure 9 shows the numerical results of the magnetic field calculated using Maxwell software. The distribution contour map of the magnetic induction intensity (B) clearly demonstrates the magnetization effect of the pole teeth. This result can be compared with the numerical results of Cheng[33] and Li[34], verifying the correctness of the magnetic field results. Figure 8c illustrates the relationship between the magnetic induction intensity at the center of the sealing gap and the axial distance. The remanent magnetic induction intensity of 1.2 T from the permanent magnet is concentrated by the pole teeth and distributed in the gap with an intensity approaching 4.0 T, which is used to confine the ferrofluid. Using the ferrofluid sealing pressure formula (Equation (4)), the total pressure resistance capability of the four-level ferrofluid sealing device can be calculated. Here, the difference between the peak and trough values of the magnetic induction intensity is 3.3 T, and the saturation magnetization strength (Ms) of the magnetic fluid is taken as 40 kA/m. Consequently, the total sealing capacity Δp is calculated to be 5.28×10^5 Pa, which far exceeds the pressure peak at the centrifugal pump shaft seal position of 33.25×10^5 Pa. Thus, the magnetic fluid sealing device designed in this work meets expectations.

$$\Delta p = \int_{B_1}^{B_2} M_s \mathrm{d}B \tag{4}$$

3.4 Magnetic field-flow field coupling simulation method

To jointly solve the problems of the morphological characteristics and failure mechanisms of ferromagnetic fluid seals using Maxwell's software and Fluent, we apply a data transfer method based on nodal interpolation and sorting techniques proposed by Li et al.[9], as illustrated in Figure 10. Additionally, the Volume of Fluid (VOF) model and the initial marker method are employed to determine the initial position of the magnetic fluid, as shown in Figure 10a, where the effect of the magnetic field on the magnetic fluid is achieved by adding a magnetic dipole force to the momentum equation source term. The expressions for the dynamic source terms of the ferromagnetic fluid in different directions are as follows:

$$f_x = M_s\left(\frac{\partial B}{\partial x}\right) \tag{5}$$

$$f_y = M_s\left(\frac{\partial B}{\partial y}\right) \tag{6}$$

where, f_x and f_y represent the components of the magnetic dipole force along the x and y directions (N/m³), respectively; while B_x and B_y denote the components of the magnetic flux density B in the x and y directions (T), respectively.

Since the volume distribution of the magnetic fluid at this time is enforced through assignment, the morphology of the ferrofluid does not have a correlation with the magnetic field forces and solid structure constraints. Therefore, the solver is changed to a transient solver with a time step of 0.0002 s, running for 20 000 steps, calculating the motion of the ferrofluid under the influence of the magnetic field over 4 s. At this moment, there is no external pressure; the inlet of the fluid domain is a pressure inlet (0 Pa) and the outlet is a pressure outlet (0 Pa).

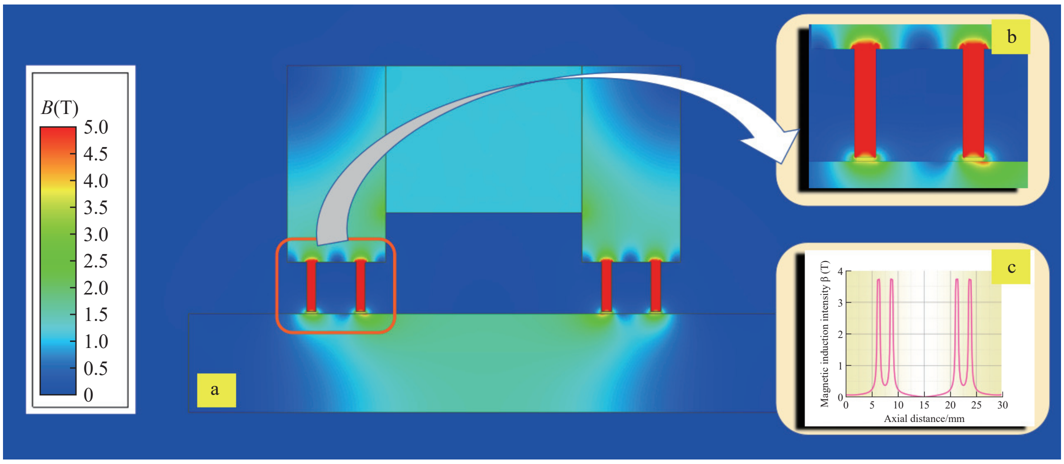

a. Distribution law of magnetic induction intensity b. Distribution law of magnetic induction intensity at the pole teeth c. The variation law of magnetic induction intensity at the sealing gap with axial distance

Figure 9 Magnetic field distribution of the ferrofluid sealing device of the centrifugal pump

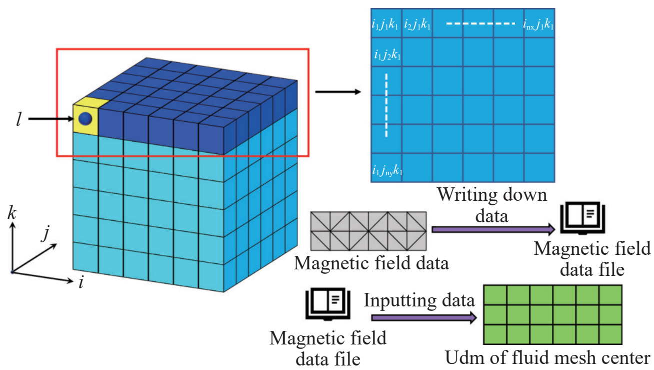

Figure 10 Principle of magnetic field-flow field interpolation[9]

As shown in Figure 11, under the action of the magnetic field force, the ferrofluid gradually transforms from its initial shape into an elliptical shape associated with the magnetic field gradient force. At 0.06 s, the initial regular shape of the ferrofluid is disrupted, and instability occurs at the interface. At 0.10 s, the ferrofluid at the upper part of the pole teeth gathers towards the bottom of the pole teeth under the influence of the magnetic field. By 1.00 s, the shape of the ferrofluid stabilizes, and the ferrofluid reaches an equilibrium state. Consequently, the morphologies of the ferrofluid at 1.00 s and 4.00 s are basically identical. Therefore, in the ferrofluid sealing device, the stable state of the ferrofluid is approximately ellipsoidal.

3.5 The influence of external pressure on the morphology of ferrofluid and the mechanism of seal failure

3.5.1 Morphological changes of ferrofluid under constant pressure

Using the computational results at t = 4 s as initial conditions, we increase the pressure value at the inlet. Initially, a constant inlet pressure boundary condition is set at 80% of the maximum pressure fluctuation P_{max} at the position P3, which corresponds to 0.3 Q_d. We observe the morphological changes of the ferrofluid under the influence of a constant external pressure P_{out}, as shown in Figure 12a.

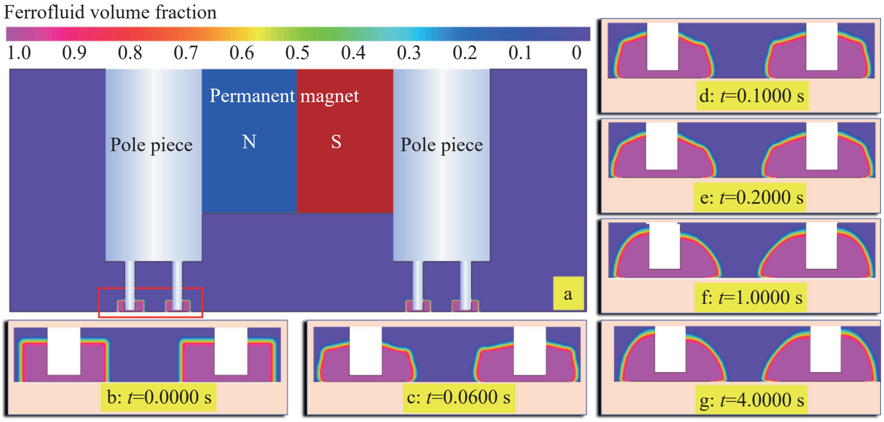

Figure 11 Morphological changes of ferrofluids under the action of a magnetic field

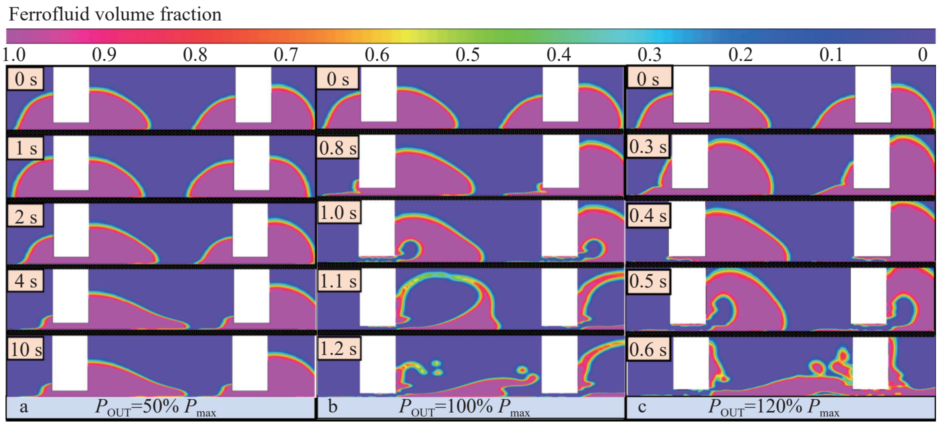

Figure 12 Ferrofluid sealing and sealing failure process

Under the action of external pressure, the original mechanical equilibrium of the ferrofluid near the pole teeth is disrupted. The ferrofluid is forced to move along the direction of the positive pressure gradient and attempts to find a new mechanical equilibrium point under the induced effect of the magnetic field. During the initial phase of action, the interface of the ferrofluid slightly deforms (at 1 s of pressure application). Subsequently, some of the ferrofluid cannot withstand the external pressure and flows toward the other side of the pole teeth along the sealing gap under the action of the positive pressure gradient (at 2 s of pressure application). As the duration of pressure application increases, the ferrofluid continues to move toward the other end of the pole teeth (from 2 to 4 s of pressure application) until the magnetic gradient force of the ferrofluid can resist the external pressure (after 4 s of pressure application), at which point no significant morphological changes or movement trajectories are observed.

Figure 12b illustrates the morphological changes of the ferrofluid when P_{out} = 100%P_{max}. Under high external pressure, the ferrofluid distributed on both sides of the pole teeth quickly passes through the sealing gap within a short time (within 1 s). Afterward, some ferrofluid remains suspended at the bottom of the pole teeth or adheres to the surface of the shaft, while a leakage channel appears at the center of the gap, accumulating a large amount of ferrofluid on the opposite side of the pole teeth, forming a hollow structure internally. With continuous pressure application, this internal hollow structure enlarges, ultimately tearing the magnetic fluid into two parts, leading to the failure of the ferrofluid seal. This result perfectly demonstrates the entire process of ferrofluid seal failure.

Figure 12c shows the morphological changes of the ferromagnetic fluid when P_{out} = 120%P_{max}. When the external pressure exceeds the maximum sealing pressure of the ferrofluid, the rupture and sealing failure processes are completed in a shorter time, with the ferrofluid sealing ring being breached within 0.6 s. However, the overall failure process is similar to that observed during the ferrofluid sealing failure process at P_{out} = 100%P_{max}.

3.5.2 Morphological changes of ferrofluid under variable pressure

In the ferrofluid seals at the shaft end of centrifugal pumps or other rotating machinery, the shaft end pressure is affected by shaft frequency and the unstable flow upstream of the sealing gap, often resulting in pressure fluctuations. There remains a research gap regarding the influence of fluctuating pressure on the interface morphology of ferrofluid seals and its effects on the sealing process. This paper employs a 3D-2D coupling method to study the sealing process of ferrofluids under the conditions of pressure fluctuations at the shaft end of the centrifugal pump.

First, the pressure results at position P3 (0.3 Q_d) at the shaft end of the centrifugal pump are extracted. Then, using boundary macro programming, real-time pressure data is recorded at the center of the inlet mesh, and new pressure data is called after each iteration, enabling the transfer of pressure results from 3D to 2D.

Figure 13 shows the morphology of the ferrofluid under average and fluctuating pressures at a flow rate of 0.3 Q_d. Within the sealing gap, the primary cause of fluctuating pressure is the rotation of the shaft surface along with the vortex motion induced by it. As a result, the amplitude of the pressure fluctuations is relatively small, and slight pressure fluctuations do not lead to the detachment of the ferrofluid structure but do accelerate the pressure breakdown process of the ferrofluid sealing ring. After 0.8 s of pressure application, there are no significant signs of rupture in the ferrofluid under average pressure, while the ferrofluid under pulsating pressure has already been extruded from the bottom of the pole teeth. Therefore, pressure fluctuations will promote the occurrence of seal failure.

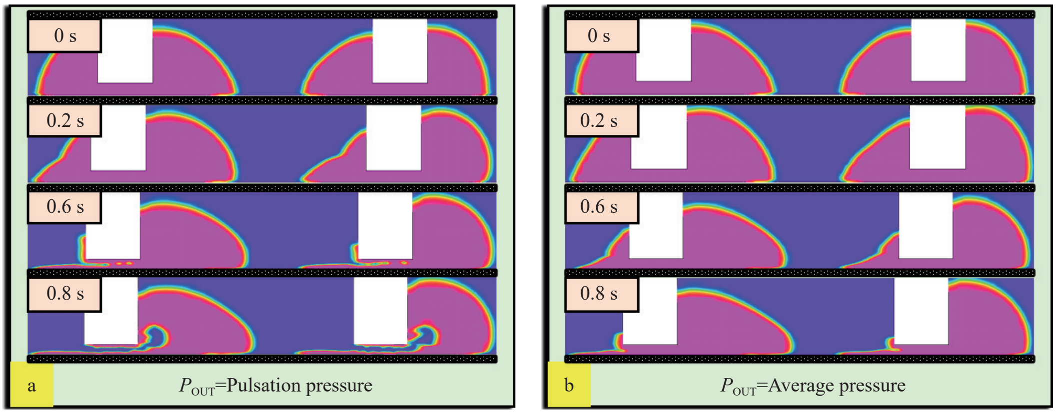

Figure 13 Variation process of the ferrofluid sealing interface under the action of pulsating pressure and average pressure

4 Conclusions

This study systematically investigated the failure mechanisms of ferrofluid seals in centrifugal pumps, with particular emphasis on the effects of pressure pulsations induced by complex flow structures in the shaft-end clearance. By establishing a coupled numerical framework integrating three-dimensional centrifugal pump simulations with two-dimensional ferrofluid sealing models, the interaction between vortex-induced pressure fluctuations and ferrofluid interface stability was quantitatively analyzed. The main conclusions can be summarized as follows:

1) Vortex dynamics in the sealing clearance are identified as the primary source of pressure pulsations at the ferrofluid sealing interface. The rotation of the pump shaft generates forced vortices near the shaft surface, while free vortices are induced in the surrounding flow field due to geometric constraints of the clearance. As the flow rate increases, especially at high-load conditions (up to 1.3 Q_d), vortex intensity and spatial complexity are significantly enhanced, leading to stronger flow instability and pressure transmission from the impeller region into the sealing gap.

2) Pressure pulsation characteristics at the ferrofluid seal interface exhibit strong dependence on operating conditions. Numerical results show that the amplitude of pressure pulsations is more pronounced under low-flow conditions, with a characteristic fluctuation magnitude of approximately 0.18 MPa. Although the absolute pressure level decreases with increasing flow rate, the unsteady pressure component remains sufficient to disturb the mechanical equilibrium of the ferrofluid sealing ring, highlighting the importance of considering transient pressure effects rather than relying solely on mean pressure design criteria.

3) A magnetic field–flow field coupling strategy was successfully developed to capture the dynamic morphology and failure process of ferrofluid seals. Under the action of the magnetic field, the ferrofluid stabilizes into an ellipsoidal configuration within the sealing gap. When subjected to increasing external pressure, the ferrofluid undergoes progressive displacement, hollow structure formation, and eventual rupture. At 100% of the maximum sealing pressure, a leakage channel forms through the center of the sealing gap, directly leading to seal failure, while higher pressures accelerate this process without fundamentally altering the failure mode.

4) Pressure pulsations do not change the failure mode of the ferrofluid seal but significantly accelerate the rupture process. Compared with constant-pressure loading, pulsating pressure causes earlier extrusion and breakdown of the ferrofluid sealing ring. Although no premature local detachment of ferrofluid is observed, the cumulative effect of pressure fluctuations reduces the effective sealing lifetime, demonstrating that unsteady flow conditions play a critical role in the reliability of ferrofluid seals in hydraulic machinery.

Overall, this work reveals the intrinsic linkage between vortex-induced pressure pulsations and ferrofluid seal failure in centrifugal pumps. The proposed multi-field coupling methodology provides a more realistic framework for evaluating ferrofluid seal performance under actual operating conditions, and the obtained insights offer valuable guidance for the structural optimization and reliability enhancement of ferrofluid sealing devices in high-speed hydraulic machinery.

Acknowledgements

This study was supported by the National Natural Science Foundation of China (Grant No. 52269022, 52379092), Innovation Fund Project for College Teachers of Gansu Province (Grant No. 2026A-029), "Kunlun Talents" Research Project (Grant No. 2023-QLGKLYCZX-032), and Science and Technology Projects of Qinghai Province (Grant No. 2025-ZJ-958M).

[References]

[1] Yang X W. Causes and fault handling of mechanical seal leakage in centrifugal pumps. Chemical Engineering and Equipment, 2023; 3: 172–174.

[2] Zhai L. Numerical simulation and experimental study on the dynamic characteristics of hermetic groove circulation labyrinth seals in centrifugal pumps. PhD dissertation. Zhejiang University, 2015; 123p.

[3] Wu M. Analysis and countermeasures of soft packing seal problems in centrifugal pumps. Manufactured and Upgraded Today, 2023; 6: 77–79, 129.

[4] Li W X, Li Z G, Han W, Li D C, Yan S N, Zhou J P. Study of the flow characteristics of pumped media in the confined morphology of a ferrofluid pump with annular microscale constraints. Journal of Fluids Engineering, 2025; 147(2): 021201.

[5] Li W X, Li Z G, Han W, Li R N, Zhang Y. Mechanism of bubble

generation in ferrofluid micro-pumps and key parameters influencing performance. Powder Technology, 2026; 467(15): 121562.

[6] Li W X, Li Z G, Han W, Wang Y, Zhao J L, Zhou J P. Morphologic transformation of ferrofluid during micropump driving under field control. Annals of the New York Academy of Sciences, 2025; 1543(1): 194–203.

[7] Chen F, Zhang J, Guo Q K, Liu Y C, Liu X B, Ding W W, et al. Carbonyl iron particles' enhanced coating effect improves magnetorheological fluid's dispersion stability. Materials, 2024; 17(18): 4449.

[8] Li W X, Li Z G, Han W, Li Y B, Yan S N, Zhao Q, et al. Measured viscosity characteristics of Fe_3O_4 ferrofluid in magnetic and thermal fields. Physics of Fluids, 2023; 35(1): 012002.

[9] Li W X, Yin J Y, Li Z G, Han W. Experimentally validated model of ferrofluid flow in micropumps. International Journal of Mechanical Sciences, 2026; 314: 111386.

[10] Nguyen D T, Nguyen N T, Nguyen M Q, Pham T T T, Le A D. Application of magnetic liquid slurries and fuzzy grey analysis in polishing nickel-phosphorus coated SKD11 steel. Particulate Science and Technology, 2022; 40(4): 401–414.

[11] Li D C, Xu H P, He X Z, Lan H Q. Study on the magnetic fluid sealing for dry Roots pump. Journal of Magnetism and Magnetic Materials, 2005; 289: 419–422.

[12] Fan D. Research on the magnetic viscosity effect of magnetic liquids at different temperatures. Beijing: Beijing Jiaotong University, 2012; 57p.

[13] Li W X, Li Z G, Zhao Q, Yan S N, Wang Z Y, Peng S Y. Influence of the solution pH on the design of a hydro-mechanical magneto-hydraulic sealing device. Engineering Failure Analysis, 2022; 135: 106091.

[14] Li Z G, Li W X, Wang Q F, Xiang R, Cheng J, Han W, et al. Effects of medium fluid cavitation on fluctuation characteristics of magnetic fluid seal interface in agricultural centrifugal pump. Int J Agric & Biol Eng, 2021; 14(6): 85–92.

[15] Liu T G, Cheng Y S, Yang Z Y. Design optimization of seal structure for sealing liquid by magnetic fluids. Journal of Magnetism and Magnetic Materials, 2005; 289: 411–414.

[16] Yoshinori M, Durst C A. Miniature magnetic fluid seal working in liquid environments. Journal of Magnetism and Magnetic Materials, 2017; 431: 285–288.

[17] Matuszewski L, Szydło Z. Life tests of a rotary single-stage magnetic-fluid seal for shipbuilding applications. Polish Maritime Research, 2011; 51–59.

[18] Szydło Z, Szczech M. Investigation of dynamic magnetic fluid seal wear process in utility water environment. Key Engineering Materials, 2012; 490: 143–155.

[19] Matuszewski L. Multi-stage magnetic-fluid seals for operating in water–life test procedure, test stand and research results, Part I: Life test procedure, test stand and instrumentation. Polish Maritime Research, 2012; 14(9): 62–70.

[20] Marcin S, Horak W. Tightness testing of rotary ferromagnetic fluid seal working in water environment. Industrial Lubrication and Tribology, 2015; 67(5): 455–459.

[21] Li X R, Fan X Q, Li Z G, Zhu M H. Failure mechanism of magnetic fluid seal for sealing liquids. Tribology International, 2023; 187: 108700.

[22] Qian J, Yang Z. Analysis of liquid-liquid interface stability of magnetic-hydraulic dynamic seals. Fluid Machinery, 2008; 36(12): 21–23, 20.

[23] Chen Y B, Li D C, Li Z K, Zhang Y J. Numerical analysis on boundary and flow regime of magnetic fluid in the sealing clearance with a rotation shaft. IEEE Transactions on Magnetics, 2018; 55(2): 1–7.

[24] Le M, Yu S, Su H, Ning Q, Zhou W. Static and rotordynamic characteristics of a sectorial labyrinth seal for centrifugal pump. Tribology International, 2025; 214: 111375.

[25] Zhou W J, Su H H, Liu H, Zhang Y, Qiu N, Gao B. Leakage and rotordynamic performance of a semi-Y labyrinth seal structure for centrifugal pump based on multi-frequency whirl method. Journal of Engineering for Gas Turbines and Power, 2025; 147(10): 101022.

[26] Xu L C, Zhang Y Q, Xu J H, Wang Y R, Chen F, Yang Y X, et al. Towards the integration of new-type power systems: Hydraulic stability analysis of pumped storage units in the S-characteristic region based on experimental and CFD studies. Energy, 2025; 329: 136755.

[27] Xu L C, Zhang Y Q, Xu J H, Zhang D S, Feng C, Zhang Z, et al. Vortex and energy characteristics in the hump region of pump-turbines based on the rigid vorticity and local hydraulic loss method. Physics of Fluids, 2025; 37(3): 035194.

[28] Ren Z P, Li D Y, Meng Z F, Liu N N, Khoo B C. Spatial-temporal correlation and fluctuating propagation characteristics of bubbles based on a coupled model of oscillation and migration. Applied Ocean Research, 2025; 161: 104677.

[29] Liang A, Chang Y Z, Zhang W W, Yao Z F, Zhu B S, Wang F J. Research on the evolution law and energy loss characteristics of rotating stall in a pump-turbine under pump mode. Energy, 2025; 330: 136696.

[30] Liang A, Zhang W W, Zhao H R, Zhou P J, Yao Z F, Zhu B S. Research on the energy loss characteristics in the double-hump region of a pump-turbine. Physics of Fluids, 2025; 37(9): 095144.

[31] Ren Z P, Li D Y, Li Z P, Wang H J, Liu J T, Li Y, et al. Absorbed-desorbed effects of ventilated pipeline. International Communications in Heat and Mass Transfer, 2025; 167(B): 109308.

[32] Li W X, Han W, Li Z G, Li R N, Zhang Y. Research on the flow rate characteristics and velocity pulsation behavior of ferrofluid micro pumps. Chemical Engineering Journal, 2025; 526: 171211.

[33] Cheng J, Li Z G, Li W X, Li X R, Gong J C. The influence of key parameters of pole teeth on the sealing pressure of the magnetohydrodynamic sealing device. Magnetic Materials and Devices, 2021; 52(5): 34–41.

[34] Li Z G, Wang M G, Chen F, Yan S N, Li W X, Cheng J. Influence of the axial tooth structure on the pressure resistance of the magnetic fluid sealing device. Vacuum, 2022; 202: 111105.